Journal of Cleaner Production 435 (2024) 140493

Contents lists available at ScienceDirect

Journal of Cleaner Production

journal homepage: www.elsevier.com/locate/jclepro

Eco-approach at an isolated actuated signalized intersection: Aware of the passing time window

Jia Hu [a], Shuoyuan Li [b], Haoran Wang [b,*], Ziran Wang [c], Matthew J. Barth [d]

[a] Key Laboratory of Road and Traffic Engineering of the Ministry of Education, Institute for Advanced Study, Tongji University, 4800 Cao'an Road, Shanghai, PR China
[b] Key Laboratory of Road and Traffic Engineering of the Ministry of Education, Tongji University, 4800 Cao'an Road, Shanghai, PR China
[c] College of Engineering, Purdue University, West Lafayette, IN, USA
[d] College of Engineering-Center for Environmental Research and Technology, University of California, Riverside, Riverside, CA, USA

ARTICLE INFO

Handling editor: Panos Seferlis

Keywords:
Eco-approach
Actuated signal timing
Chance constraint
Multivariate Markov chain
Optimal control

ABSTRACT

Isolated actuated signalized intersection is a pressing challenge for conventional eco-approach methods, due to the ever-changing signal timing strategy. This research proposes an optimal control based eco-approach method tailored to tackle this challenge. The proposed method bears the following features: i) capable of predicting the ever-changing actuated signal timing; ii) with enhanced fuel efficiency via proactively catching a feasible passing time window; iii) with real-time computation efficiency for implementation. Simulation results demonstrate that the proposed method enhances fuel efficiency by 9.1%, reduces stop count by 14.8%, and enhances safety performance by 317.14%, compared to conventional human-driven vehicles. The passing time window prediction capability is confirmed with an accuracy of 3.1 s. All the aforementioned benefit is at a cost of a minimal travel time increase of 5.5 s. Moreover, the average computation time of the proposed method is 12 ms, demonstrating its readiness for field implementation.

1. Introduction

Transportation stands as a primary contributor to global warming (Masson-Delmotte et al., 2022). It is responsible for over 27% of greenhouse gas emissions (Aminzadegan et al., 2022). Among all modes of transportation, road transportation accounts for approximately 72% of energy consumption and more than 80% of CO_2 emissions (Holmberg et al., 2012). In road transportation scenarios, approaching intersections presents a significant energy-wasting challenge, leading to the consumption of 2.8 billion gallons of gasoline in the United States alone (Davis and Boundy, 2021). To mitigate this, eco-approach technology has been developed for Connected and Automated Vehicles (CAVs), focusing on reducing fuel consumption by avoiding inefficient stop-and-go patterns (Wang et al., 2022d).

Conventional eco-approach studies mainly focus on the fixed signalized intersection, employing two main planning methods: Reinforcement Learning (RL) and optimal control. RL methods compute driving behaviors by training agents to interact with the environment. Initial research in this domain utilized Q-learning (Fei Ye et al., 2019), an RL method based on value estimation in discrete action spaces. However, the discrete nature of Q-learning limits its applicability in scenarios requiring continuous action space. To overcome this limitation, recent advancements have shifted towards policy-based RL methods designed for continuous action spaces in eco-driving applications (Vindula Jayawardana, 2022). For instance, Guo et al. implemented the Deep Deterministic Policy Gradient (DDPG) algorithm, integrating both longitudinal acceleration and lateral lane-changing decisions (Guo et al., 2021). Similarly, Zhang et al. developed an eco-driving approach utilizing the Twin Delayed Deep Deterministic (TD3) policy gradient algorithm (Zhang et al., 2022). While these policy-based methods are noted for their computational efficiency, their training processes often lack transparency and fail to account for vehicle dynamics (Li, 2017). This opacity can result in actions that exceed the vehicle's operational capabilities or compromise safety. Consequently, potential safety risks and execution failures remains a critical concern in the application of RL methods in eco-driving scenarios.

Optimal control methods focus on solving optimization problems aimed at minimizing fuel consumption. These methods typically employ a vehicle kinematics model (Wang et al., 2023) or a vehicle dynamics model (Jia et al., 2022). The precision of these models mitigates

* Corresponding author.
E-mail addresses: hujia@tongji.edu.cn (J. Hu), shuoyuanli@tongji.edu.cn (S. Li), wang_haoran@tongji.edu.cn (H. Wang), ryanwang11@hotmail.com (Z. Wang), matthew.barth@ucr.edu (M.J. Barth).

https://doi.org/10.1016/j.jclepro.2023.140493
Received 8 October 2023; Received in revised form 9 December 2023; Accepted 29 December 2023
Available online 1 January 2024

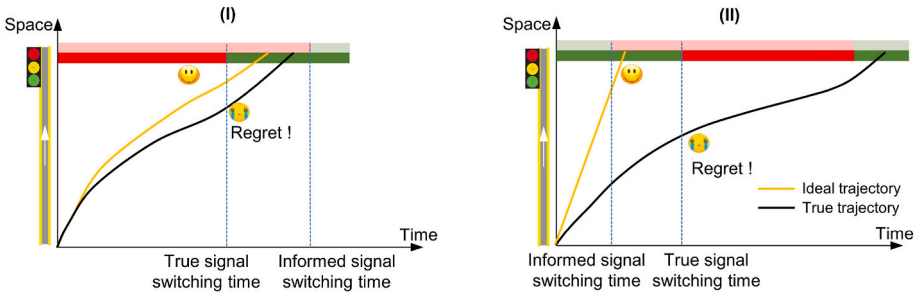

Fig. 1. Eco-approach at actuated signalized intersection: dynamic signal timing.

concerns related to tracking errors during execution, making optimal control a preferred approach in numerous eco-approach studies. A significant advancement in the domain of eco-approach controllers is the introduction of overtaking capabilities by (Hu et al., 2021). Their model distinctively considers the stochastic nature of surrounding traffic, marking a noteworthy development in this area. Further building on this, Hu et al. refined this model, positioning it as one of the few methods integrating lane-level navigation features (Hu et al., 2023). Based on Hu et al.'s optimal control framework, this paper addresses the unique challenges inherent to actuated signalized intersections. Additionally, Dong et al. proposed an eco-approach controller that considers the queue of vehicles ahead, enhancing practical applicability (Dong et al., 2021). This research was further extended to multi-intersection scenarios and evaluated in real-world settings (Dong et al., 2022). Yang et al. developed a strategy for ecological speed guidance in vehicle platoons (Yang et al., 2020), and Lei et al. proposed a dynamic inverse hierarchical optimization method specifically tailored for hybrid electric vehicles (Lei et al., 2023). Given the extensive research and successful field tests, the optimal control method has emerged as a promising strategy for eco-approach applications, offering a blend of accuracy, practicality, and adaptability to diverse driving scenarios.

However, conventional eco-approach controllers encounter significant challenges at an actuated signalized intersection which is widely deployed on urban roads. Unlike the fixed signal timing, actuated signal controller is a more flexible way, characterized by its dynamic signal timings in response to real-time traffic status. In such environments, traditional controllers an unaware of the remaining time (time to signal switching) of an actuated signal. Hence, ecological approaching trajectories are no more obtained. For example, as illustrated in Fig. 1-(I), a CAV approaching a red signal might decelerate in anticipation of a prolonged stop, only to find the signal turning green prematurely. Conversely, as depicted in Fig. 1-(II), a CAV might slow down during a green phase based on outdated information, potentially missing the opportunity to cross the intersection.

In addressing the challenge of eco-approach at an isolated actuated signalized intersection, early studies aimed to adapt the problem to the conventional eco-approach scenarios at fixed signalized intersections by estimating a probable signal timing for ecological trajectory planning. For instance, Hao et al. approached this by calculating the remaining duration of the current signal phase as the average of the minimum and maximum values obtained from the signal controller (Hao et al., 2019). Similarly, Shafik et al. estimated the signal switching time (from red to green) by randomly sampling from a Gaussian distribution modeled from historical signal timing data (Shafik et al., 2023). Broek et al. determined the optimal passing time for the ego-vehicle through the intersection based on the moment with the highest probability of encountering a green light, as inferred from historical data (Borek et al., 2022). Despite these innovative approaches, a common limitation emerges: the inability to consistently plan optimal eco-approach maneuvers. This stems from the reliance on predetermined signal timings, which may not always align with real-time conditions, leading to potential misjudgments. Recognizing this issue, Sun et al. developed an eco-approach controller based on robust optimization (Sun et al., 2020), incorporating a chance constraint on the vehicle's arrival time relative to the uncertain signal timings represented by a Gaussian distribution. Yet, this method, too, depends on historical data and does not fully account for real-time traffic dynamics. These observations highlight an ongoing need for an effective eco-approach controller specifically tailored for isolated actuated signalized intersections, one that can dynamically adapt to signal timing variations in accordance to real-time traffic conditions.

In this paper, a novel eco-approach method is specifically designed for an isolated actuated signalized intersection to ensure ecological driving. This method stands out with several key contributions:

- **Predictive Capability for Actuated Signal Timing**: Utilizing the Markov Process (MP), this research is adept at predicting the future state of an actuated signal controller. Traffic conditions are innovatively integrated as a state transition variable in Multivariate Markov Chains (MMCs), bolstering the accuracy of signal timing predictions. This predictive capability is crucial in adapting to the dynamic nature of actuated signalized intersections.
- **Enhanced Fuel Efficiency at Actuated Intersections**: Based on the forecasted actuated signal timing, the proposed method is capable of predicting feasible passing time windows. The passing time window prediction facilitates the proactive behaving of ego-vehicle in anticipation of future signal changes. Hence, the proposed method reduces unnecessary stops and speed oscillations, thereby enhancing fuel efficiency.
- **Real-time Computational Efficiency**: In addressing the challenges of computational complexity, the chance constraint of passing time window within the optimal control problem has been linearized. This significantly streamlines the computational process. Furthermore, we have implemented a dynamic programming-based algorithm,

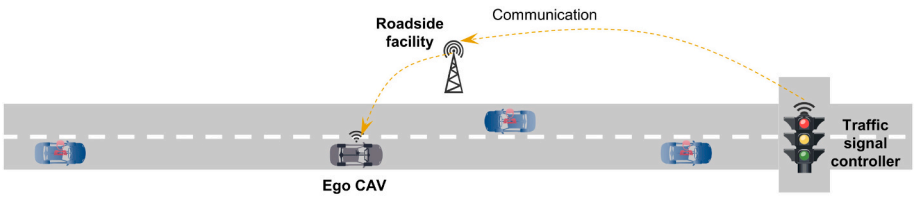

Fig. 2. The scenario of interest: an isolated actuated signalized intersection.

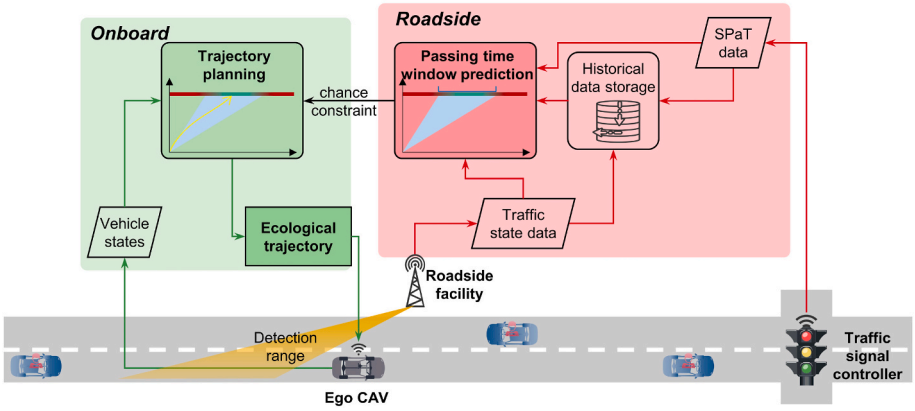

Fig. 3. Structure of the proposed eco-approach controller at an isolated actuated signalized intersection.

facilitating the real-time resolution of a quadratic Model Predictive Control (MPC) problem. This design enhances the practicality of the controller in real-time scenarios.

2. Methodology

2.1. Scenario of interest

A typical application scenario of the proposed eco-approach controller is shown in Fig. 2, where an isolated actuated signal controller prioritizes the main road, and a single CAV on the main road, equipped with the proposed controller, aims to pass through the intersection ecologically. The CAV communicates with roadside facilities to receive passing time window navigations and then plans eco-approach trajectories. The proposed controller is without the consideration of the CAV penetration rate.

2.2. System structure

The system structure of the proposed eco-approach method is illustrated in Fig. 3. The eco-approach system is implemented both onboard and on the roadside. The control logic is described as follows.

- **Roadside module**: Within the roadside module, crucial data is collected to facilitate eco-approach maneuvers. This module gathers real-time Signal Phase and Timing (SPaT) information (including current signal time, current signal phase, phase setting, and circle length) directly from the traffic signal controller, alongside real-time traffic state data obtained from roadside sensing facilities, which may include advanced technologies such as video and radar sensors. Both real-time SPaT data and traffic state data are stored as historical data. Leveraging historical and real-time datasets, a dedicated passing time window prediction method is developed. The passing time window is an accumulation of the feasible passing timing. It serves as a dynamic chance constraint when planning the trajectory of the eco-approach, ensuring adaptability to actuated signal timing.
- **Onboard module**: Within the onboard module, a trajectory planner is proposed to address the eco-approach problem. This module capitalizes on the passing time window prediction output, treating it as a vital chance constraint. Taking real-time vehicle states into account, the system generates ecological trajectories tailored for the ego-CAV to execute. This approach ensures that the vehicle responds dynamically to actuated signal timing while adhering to eco-friendly principles.

2.3. Problem formulation

The proposed eco-approach controller is designed as a Chance Constrained Model Predictive Control (CCMPC) problem. This framework effectively manages the inherent uncertainty associated with actuated signal timing by incorporating a meticulously crafted chance constraint. This chance constraint is derived from the prediction of passing time window which uses the Markov Process (MP) as a basis. The detailed formulation and workings of this controller are thoroughly expounded upon in the subsequent sections of this paper.

2.3.1. System definition

The mathematical definition of the proposed eco-approach system is provided as follows.

Roadside state $\boldsymbol{\xi}^R$ includes the state of traffic and signal. It is perceived via roadside facilities, as shown in Fig. 4.

$$\boldsymbol{\xi}^R(t) \overset{\text{def}}{=} [x_s(t), x_{c_1}(t), x_{c_2}(t), \cdots, x_{c_i}(t), \cdots, x_{c_N}(t)]^T \tag{1}$$

where t is the signal time, $t \in \{0, 1, 2, \ldots, T-1\}$; T is the length of a signal cycle; $x_s(t)$ is the state of signal defined as equation (2). It is provided by SPaT from the signal controller. The state of traffic $x_{c_i}(t)$ is detected by roadside facility. Its detection region is partitioned into cells, as illustrated in Fig. 4. The traffic state is defined based on the occupancy of these smaller cells as equation (3).

$$x_s(t) \overset{\text{def}}{=} \begin{cases} 0 & \text{signal is not green} \\ 1 & \text{signal is green} \end{cases} \tag{2}$$

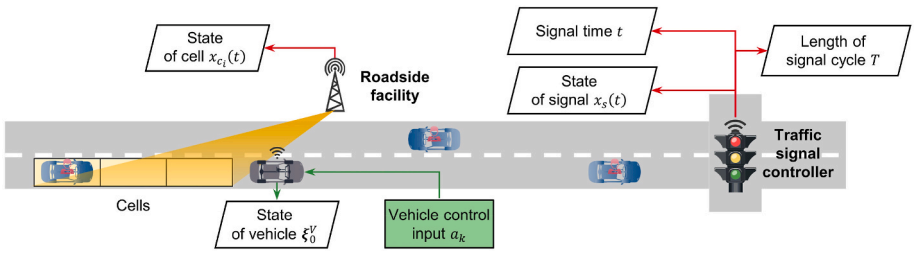

Fig. 4. System states declaration.

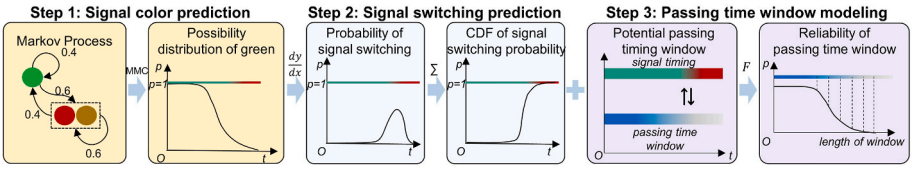

Fig. 5. The prediction process of passing time window.

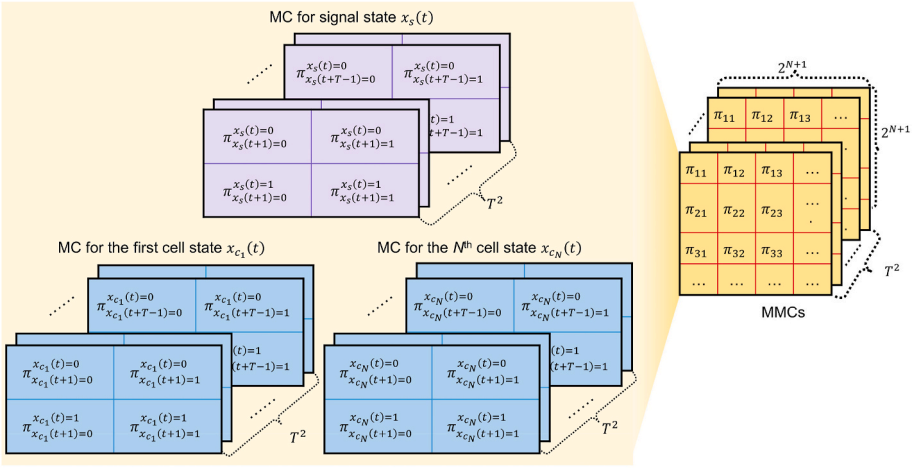

Fig. 6. MMCs for signal color prediction. (For interpretation of the references to color in this figure legend, the reader is referred to the Web version of this article.)

$$x_{c_i}(t) \overset{\text{def}}{=} \begin{cases} 0 & \text{there is no vehicle in cell } i \\ 1 & \text{there is vehicle in cell } i \end{cases} \tag{3}$$

where i is the index of the cell, $i \in \{0, 1, 2, \ldots, N\}$. N is the number of cells.

Onboard vehicle state $\boldsymbol{\xi}_k^V$ and control variable u_k are defined as follows.

$$\boldsymbol{\xi}_k^V \overset{\text{def}}{=} \begin{bmatrix} s_k \\ v_k \end{bmatrix} \tag{4}$$

$$u_k \overset{\text{def}}{=} a_k \tag{5}$$

where s_k is the longitudinal position of ego-CAV; v_k the speed of ego-CAV; a_k is the acceleration of ego-CAV; k is the control time step index, $k \in \{1, 2, \ldots, K\}$; K is the number of control steps.

2.3.2. Passing time window prediction

To enable an eco-approach at an isolated actuated signalized intersection, the ego-CAV must make optimal decisions regarding the passing timing at the stop line. However, the feasible passing timing through the intersection is inherently uncertain due to the ever-changing actuated signal timing. Therefore, this paper introduces a methodology to identify feasible passing timing and formulate it into a potential passing time window. The prediction process of the passing time window is summarized in Fig. 5 and elaborated upon as follows:

Step 1 (Signal color prediction): In this initial step, predictions are made regarding the likelihood that the signal light will be green, based on a combination of historical and real-time data of both signal state and traffic state. These predictions are derived using a Markov Process (MP) model, resulting in the creation of a Possibility Distribution Function (PDF) representing the probability of a green light.
Step 2 (Signal switching prediction): The signal switching time is the signal time when signal color changes. The signal switching probability is a differential of the PDF of the green light. The signal switching prediction finally outputs a Cumulative Distribution Function (CDF) of signal switching probability.
Step 3 (Passing time window modeling): The concept of a passing time window is defined as an accumulation of feasible passing timing. The reliability of a passing time window is quantified as the probability that the actual passing time window has a wider range than the identified time window. It is realized via the CDF of signal switching probability.

2.3.2.1. Signal color prediction.

The color of an actuated traffic signal controller is predicted via the Markov Process (MP) (Gagniuc, 2017). In this paper, the approach goes further by formulating Multivariate Markov Chains (MMCs). These MMCs are designed to take into account not only the signal state but also the traffic state in the prediction process. This enhanced modeling approach enables a more comprehensive and accurate prediction of signal color, considering both the dynamic changes in signal state and concurrent variations in traffic conditions.

To cover both traffic and signal status, all relevant variables in $\boldsymbol{\xi}^R(t)$ are adopted for the prediction process. For each variable, its transition is modeled using a Markov Chain (MC), as illustrated in Fig. 6. Each MC comprises an accumulation of transition matrices. The transition probability in the matrices is calculated as follows:

$$\pi_{x_*(t+\Delta t)}^{x_*(t)} = \frac{H_{x_*(t+\Delta t)}^{x_*(t)}}{H^{x_*(t)}}, * \in \{s, c_i\} \tag{6}$$

where $x_*(t)$ is a roadside state variable in $\boldsymbol{\xi}^R(t)$; Δt is a transition horizon; $H^{x_*(t)}$ is the number of occurrences of $x_*(t)$ in the historical data set; $H_{x_*(t+\Delta t)}^{x_*(t)}$ is the number of transitions from $x_*(t)$ to $x_*(t+\Delta t)$ in the historical data set.

By integrating all individual MCs, MMCs are formulated into the Cartesian product of MCs (Shin and Sunwoo, 2018), as illustrated in Fig. 6. The resulting MMCs are then organized into a series of multivariate transition matrices. It consists of T^2 transition matrices, each

with a size of $2^{N+1} \times 2^{N+1}$.

Leveraging the MMCs, it becomes possible to predict the probability of transiting from one state to another in the future. Specifically, at time t, the prediction result of the MMCs is the probability of observing a green light after time duration Δt, denoted as $p^G_{t+\Delta t}$. A discussion on this probability is presented as follows.

$p^G_{t+\Delta t}$ is transformed into the discretized horizon to adapt to the context of trajectory planning. To clarify, let the current signal time be t and the control step size be $\Delta\tau$, and the control step at k correspond to time $t + k\Delta\tau$. Consequently, the probability of encountering a green light at control step k is calculated using equation (7).

$$p^G_k = p^G_{t+k\Delta\tau} \tag{7}$$

By defining the event A^G_k as observing a green light at step k, $p^G_k = Pr(A^G_k)$. Considering the signal phasing strategy, as presented in equation (8), A^G_k occurring means the occurring of $A^G_1 \cdots A^G_{k-2}, A^G_{k-1}$, when current signal is green. Moreover, A^G_k occurring also indicates the occurring of $A^G_{k+1}, A^G_{k+2} \cdots A^G_{\widetilde{K}}$, when current signal is red.

$$Pr\left(A^G_k\right) = \begin{cases} Pr\left(A^G_1 \cup A^G_2 \cup \cdots \cup A^G_k\right) & x_s(t) = 1 \\ Pr\left(A^G_k \cup A^G_{k+1} \cup \cdots \cup A^G_{\widetilde{K}}\right) & x_s(t) = 0 \end{cases} \tag{8}$$

where $\widetilde{K}$ is the signal time of the prediction horizon, $\widetilde{K} \le K$. It is generally set to the step when signal color is determined, such as the middle of a signal phase, to ensure the prediction only covers one time of signal color switching.

2.3.2.2. Signal switching prediction. MMCs have provided forecasts of the likelihood of a green traffic signal p^G_k. The signal switching probability at a specific step, denoted as $p^S_{k_{sw}}$, can be determined according to equation (9).

$$p^S_{k_{sw}} = \begin{cases} Pr\left(A^G_{k_{sw}-1} \cap \overline{A}^G_{k_{sw}}\right) & x_s(t) = 1 \\ Pr\left(\overline{A}^G_{k_{sw}-1} \cap A^G_{k_{sw}}\right) & x_s(t) = 0 \end{cases} \tag{9}$$

where k_{sw} is the signal-switching step; $\overline{A}^G_{k_{sw}}$ is the opposite event that the signal is not green at step k_{sw}.

By applying equation (8) to equation (9), equation (10) is obtained.

$$p^S_{k_{sw}} = \begin{cases} p^G_{k_{sw}-1} - p^G_{k_{sw}} & x_s(t) = 1 \\ p^G_{k_{sw}+1} - p^G_{k_{sw}} & x_s(t) = 0 \end{cases} \tag{10}$$

Moving forward, the probability of signal switching event occurring within the K_{sw} steps is denoted as $P^S_{K_{sw}}$. It is the Cumulative Distribution Function (CDF) of $p^S_{k_{sw}}$ over a sequence of K_{sw} as equation (11).

$$P^S_{K_{sw}} = F_{k_{sw}}(K_{sw}) = Pr(k_{sw} \le K_{sw}) = \sum\nolimits_{k_{sw}=1}^{k_{sw}=K_{sw}} p^S_{k_{sw}} \tag{11}$$

2.3.2.3. Passing time window modeling. At the present signal time t, the identified passing time window $\mathbf{K}_{pass}$ is defined as a collection of planning steps ahead of or after the signal-switching step, as shown in equation (12). Here, $\mathbf{K}_{pass}$ is also discussed according to different signal colors at the current time.

$$\mathbf{K}_{pass} = \begin{cases} \mathbf{K}^G_{pass} = \{k | 1 \le k \le \widetilde{k}_{sw}\} & x_s(t) = 1 \\ \mathbf{K}^R_{pass} = \{k | \widetilde{k}_{sw} \le k \le K\} & x_s(t) = 0 \end{cases} \tag{12}$$

where $\widetilde{k}_{sw}$ is the predicted signal-switching step. $\mathbf{K}^G_{pass}$ is the passing time window in a green phase; $\mathbf{K}^R_{pass}$ is the passing time window in a red phase.

The reliability of the identified passing time window is quantified by the probability that the actual passing time window has a wider range than the identified passing time window, denoted as $Pr(\mathbf{K}_{pass})$ in equation (13). It is contingent on the CDF $F_{k_{sw}}(K_{sw})$ in equation (11). The reliability of the identified passing time window indicates the passing success rate for ego-CAV when it arrives at the intersection within the identified passing time window.

$$Pr(\mathbf{K}_{pass}) = \begin{cases} Pr\left(\mathbf{K}^G_{pass}\right) = Pr(k_{sw} \ge \widetilde{k}_{sw}) = 1 - F_{k_{sw}}(\widetilde{k}_{sw}) & x_s(t) = 1 \\ Pr\left(\mathbf{K}^R_{pass}\right) = Pr(k_{sw} \le \widetilde{k}_{sw}) = F_{k_{sw}}(\widetilde{k}_{sw}) & x_s(t) = 0 \end{cases} \tag{13}$$

2.3.3. Trajectory planning

To compute an eco-approach maneuver for the ego-CAV, trajectory planning is cast as a Chance Constrained Model Predictive Control (CCMPC) problem (Wang et al., 2022a). This approach leverages the distribution of passing time window as a chance constraint to regulate the ego-CAV's arrival time at the intersection, thereby allowing users to personalize the trade-off between mobility and reliability.

2.3.3.1. Cost function. The CCMPC cost function takes a quadratic form, as expressed in equation (14). It seeks to minimize a composite cost that comprises three components: state error cost, fuel cost, and terminal state error cost. Since actual fuel consumption model is non-convex and could substantially increase computational complexity, the square of acceleration is employed as a proxy for fuel cost. The cost function is designed to strike a balance between fuel efficiency and vehicular mobility.

$$\min_{u} \left(\sum\nolimits_{k=0}^{K-1} \left(\underbrace{\frac{1}{2}\left(\boldsymbol{\xi}^V_k - \boldsymbol{\xi}^V_{des,k}\right)^T \boldsymbol{Q} \left(\boldsymbol{\xi}^V_k - \boldsymbol{\xi}^V_{des,k}\right)}_{\text{State error cost}} + \underbrace{\frac{1}{2} u_k^T R u_k}_{\text{Fuel cost}} \right) + \underbrace{\frac{1}{2}\left(\boldsymbol{\xi}^V_K - \boldsymbol{\xi}^V_{des,K}\right)^T \boldsymbol{Q} \left(\boldsymbol{\xi}^V_K - \boldsymbol{\xi}^V_{des,K}\right)}_{\text{Terminal state error cost}} \right) \tag{14}$$

where $\boldsymbol{Q} \overset{\text{def}}{=} \text{diag}(0, q_v)$; q_v is the weighting factor of longitudinal speed error cost; R is the weighting factor of acceleration cost. They are used to adjust the importance of each cost component. $\boldsymbol{\xi}^V_{des,k} \overset{\text{def}}{=} \begin{bmatrix} s_{des} \\ v_{des} \end{bmatrix}$ is the desired vehicle state at step k; Notably, the desired position s_{des} is excluded due to its zero-cost weighting. v_{des} is the desired driving speed.

2.3.3.2. Vehicle dynamics. The motion of the ego-CAV follows a vehicle dynamics model formulated based on kinematics (Wang et al., 2022c), as presented in equation (15). This model utilizes matrices $\boldsymbol{A}$ and $\boldsymbol{B}$ to describe the vehicle's state evolution over time.

$$\boldsymbol{\xi}^V_{k+1} = \boldsymbol{A}\boldsymbol{\xi}^V_k + \boldsymbol{B}u_k \tag{15}$$

$$\boldsymbol{A} = \begin{bmatrix} 1 & \Delta\tau \\ 0 & 1 \end{bmatrix} \tag{16}$$

$$\boldsymbol{B} = \begin{bmatrix} \frac{\Delta\tau^2}{2} \\ \Delta\tau \end{bmatrix} \tag{17}$$

where $\Delta\tau$ is the length of a control time step.

2.3.3.3. Constraints

2.3.3.3.1. Passing time window constraint. The ego-CAV is required to cross the stop-line within a user preferred passing time window:

$$\begin{cases} s_k > s_{stop} & x_s(t) = 1, k \in \mathbf{K}^G_{pass} \\ s_k < s_{stop} & x_s(t) = 0, k \in \mathbf{K}^R_{pass} \end{cases} \tag{18}$$

Algorithm 2: Solution algorithm of the proposed eco-approach controller

Input: initial state $\boldsymbol{\xi}_0^V$, desired state $\boldsymbol{\xi}_{des,k}^V$, number of control steps K, $\boldsymbol{A}$, $\boldsymbol{B}$, $\boldsymbol{Q}$, R

Output: optimal control u_k and state $\boldsymbol{\xi}_k^V$ for each step

Initialize: $iter = 0$

while $\left\|\boldsymbol{u}^{iter} - \boldsymbol{u}^{iter-1}\right\| > \varepsilon$ **do**

$iter = iter + 1$

$\widetilde{\boldsymbol{Q}}_K \triangleq^{\text{def}} \boldsymbol{Q}$

$\widetilde{\boldsymbol{D}}_K \triangleq^{\text{def}} -\boldsymbol{Q}\boldsymbol{\xi}_{des,k}^V$

For $k \in \{K-1, \cdots, 1\}$

$\boldsymbol{D}_k = -\boldsymbol{Q}\boldsymbol{\xi}_{des_i}$

$\widetilde{\boldsymbol{Q}}_k = \boldsymbol{G}_k^T \boldsymbol{R}_k \boldsymbol{G}_k + \boldsymbol{S}_k^T \widetilde{\boldsymbol{Q}}_{k+1} \boldsymbol{S}_k + \boldsymbol{Q}$

$\widetilde{\boldsymbol{D}}_k = \boldsymbol{G}_k^T \boldsymbol{R}_k \boldsymbol{H}_k + \boldsymbol{S}_k^T \widetilde{\boldsymbol{Q}}_{k+1} \boldsymbol{T}_k + \boldsymbol{S}_k^T \widetilde{\boldsymbol{D}}_{k+1}$

$\boldsymbol{P}_k = (\boldsymbol{R}_k + \boldsymbol{B}_k^T \widetilde{\boldsymbol{Q}}_{k+1} \boldsymbol{B}_k)^{-1}$

$\boldsymbol{G}_k = -\boldsymbol{P}_k \boldsymbol{B}_k^T \widetilde{\boldsymbol{Q}}_{k+1} \boldsymbol{A}_k$

$\boldsymbol{H}_k = -\boldsymbol{P}_k \boldsymbol{B}_k^T \left(\widetilde{\boldsymbol{Q}}_{k+1} + \widetilde{\boldsymbol{D}}_{k+1}\right)$

$\boldsymbol{T}_k = \boldsymbol{B}_k \boldsymbol{H}_k$

$\boldsymbol{S}_k = \boldsymbol{A}_k + \boldsymbol{B}_k \boldsymbol{G}_k$

For $k \in \{0, 1, \cdots, K\}$

$u_k = \boldsymbol{G}_k \boldsymbol{\xi}_k^V + \boldsymbol{H}_k$

$\boldsymbol{\xi}_{k+1}^V = \boldsymbol{S}_k \boldsymbol{\xi}_k^V + \boldsymbol{T}_k$

if $\boldsymbol{\xi}^{V,iter} > \boldsymbol{\xi}_{max}^V$ **then**

$\boldsymbol{\xi}^{V,iter} = \boldsymbol{\xi}_{max}^V$

if $\boldsymbol{\xi}^{V,iter} < \boldsymbol{\xi}_{min}^V$ **then**

$\boldsymbol{\xi}^{iter} = \boldsymbol{\xi}_{min}^V$

if $\boldsymbol{u}^{iter} > \boldsymbol{u}_{max}$ **then**

$\boldsymbol{u}^{iter} = \boldsymbol{u}_{max}$

if $\boldsymbol{u}^{iter} < \boldsymbol{u}_{min}$ **then**

$\boldsymbol{u}^{iter} = \boldsymbol{u}_{min}$

However, due to the uncertainty of the passing time window as determined in equation (13), this constraint is reformulated into a chance constraint, as articulated in equation (19).

$$\begin{cases} Pr\left(s_k > s_{stop}\right) \geq \gamma & x_s(t) = 1, k \in \mathbf{K}_{pass}^{G} \\ Pr\left(s_k < s_{stop}\right) \geq \gamma & x_s(t) = 0, k \in \mathbf{K}_{pass}^{R} \end{cases} \tag{19}$$

where γ is a risk parameter, $\gamma \in (0,1)$. It allows users to specify their desired level of risk. In this research, γ is set to 0.5.

Constraint (19) indicates that the user preferred passing window $\mathbf{K}_{pass}$ should be determined to satisfy the risk parameter γ as follows.

$$\begin{cases} Pr\left(\mathbf{K}_{pass}^{G}\right) \geq \gamma & x_s(t) = 1 \\ Pr\left(\mathbf{K}_{pass}^{R}\right) \geq \gamma & x_s(t) = 0 \end{cases} \tag{20}$$

By applying equation (13) into equation (20), the signal switching time could be clarified as follows.

$$\begin{cases} \widetilde{k}_{sw} = F_{k_{sw}}^{-1}(1-\gamma) & x_s(t) = 1 \\ \widetilde{k}_{sw} = F_{k_{sw}}^{-1}(\gamma) & x_s(t) = 0 \end{cases} \tag{21}$$

Hence, the chance constraint (19) could be linearized by applying equation (21) as follows.

$$\begin{cases} s_k > s_{stop} & x_s(\widetilde{t}) = 1, k \in \left\{K - F_{k_{sw}}^{-1}(1-\gamma), K - F_{k_{sw}}^{-1}(1-\gamma) + 1, \ldots, K\right\} \\ s_k < s_{stop} & x_s(\widetilde{t}) = 0, k \in \left\{1, \ldots, F_{k_{sw}}^{-1}(\gamma)\right\} \end{cases} \tag{22}$$

2.3.3.3.2. Collision avoidance constraints. Collision avoidance between the ego-CAV and its preceding vehicle is achieved by regulating the car-following gap:

$$s_k \leq s_k^{front} - s_{safe} \tag{23}$$

where s_{safe} is the minimum safe car-following gap, which is set to 5 m in this research. s_k^{front} is the longitudinal position of the preceding vehicle at step k. The prediction of the preceding vehicle's actions is computed based on a logical assessment of potential future behaviors under varying traffic signal conditions. This prediction process is formulated as follows:

$$a_k^{front} = \begin{cases} a_{acc} & x_s(\widetilde{t} + k\Delta\tau) = 1 \ and \ v_k^{front} < v_{tra} \\ a_{dec} & x_s(\widetilde{t} + k\Delta\tau) = 0 \\ 0 & else \end{cases} \tag{24}$$

where a_k^{front} is the acceleration of the preceding vehicle at step k; a_{acc} is the acceleration of a speed-up action; a_{dec} is the acceleration of a slow-down action; v_k^{front} is the speed of the preceding vehicle; v_{tra} is the average speed of traffic. The decision to speed up is predicted when the traffic signal is green and the preceding vehicle's speed is less than the average traffic speed. Conversely, slowing down is anticipated when the traffic signal is red. In all other scenarios, the preceding vehicle is expected to maintain a constant speed. The values of a_{acc} and a_{dec} can be empirically determined from field trajectory data.

2.3.3.3.3. Execution capability constraints. The vehicle's speed and acceleration must adhere to certain limits as follows.

$$0 \leq v_k \leq v_{max} \tag{25}$$

$$a_{min} \leq a_k \leq a_{max} \tag{26}$$

where v_{max} is the speed limit, a_{min} and a_{max} are the minimum and maximum accelerations, respectively.

2.3.3.3.4. Solution algorithm. The linearized CCMPC problem is tackled using a dynamic programming-based algorithm developed by the authors (Wang et al., 2022b). This algorithm efficiently computes the optimal solution through backward calculations involving concomitant matrices and forward calculations involving control and state vectors. By predefining the optimal terminal state, this approach enhances computational efficiency. The algorithm's detailed procedure is outlined below.

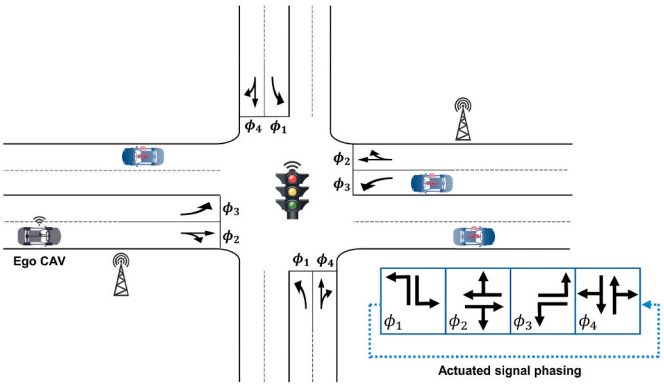

Fig. 7. Test scenario.

Table 1
Parameters setting.

Name	Definition	Value
T	Cycle length of the actuated traffic signal controller	160 s
$G_{\varphi_j}^{min}$	Minimum duration of the φ_j signal phase	$G_{\varphi_1}^{min} = 15$ s $G_{\varphi_2}^{min} = 20$ s $G_{\varphi_3}^{min} = 20$ s $G_{\varphi_4}^{min} = 15$ s
$G_{\varphi_j}^{max}$	Maximum duration of the φ_j signal phase	$G_{\varphi_2}^{max} = 50$ s $G_{\varphi_3}^{max} = 40$ s
T_A	Duration of yellow	3 s
T_r	Duration of red clearance	2 s
q_J	The volume of the vehicle from J entry of the intersection	$q_J \leq cap_J$
cap_J	The road capacity of the J entry of the intersection.	1200 pcu/h
D_{eco}	Distance of the range for eco-approach	500 m

Table 2
Case definition.

	$v/c = 0.1$	$v/c = 0.3$	$v/c = 0.5$	$v/c = 0.7$	$v/c = 0.9$
$v_{max} = 60km/h$	Case 1	Case 2	Case 3	Case 4	Case 5

Two types of eco-approach controllers are evaluated.

3. Evaluations

The proposed eco-approach controller is evaluated via simulations on the VISSIM platform. The evaluation is conducted from the following perspectives: i) function validation; ii) passing time window prediction; iii) fuel-efficiency; iv) driving mobility; v) driving safety; vi) computational efficiency; vii) parameter tuning.

3.1. Test scenario

The test scenario is illustrated in Fig. 7. In this scenario, the ego-CAV would like to ecologically pass through an isolated actuated signalized intersection. Notably, the ego-CAV is traversing along the main branch, and it is given with the priority by the signal controller's configuration. The actuated signal timing logic for this scenario is outlined in Fig. 7. Essential parameters for the actuated signal timing are provided in Table 1.

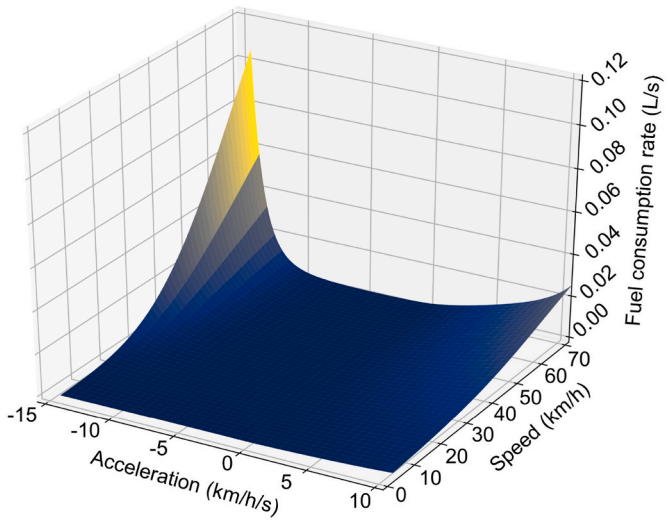

Fig. 8. Vehicle fuel consumption rate.

3.2. Experiment design

To evaluate the proposed eco-approach controller, five cases are designed as illustrated in Table 2. They cover different congestion levels, quantified by volume-to-capacity ratio: v/c. The traffic speed limit is set to $60km/h$. In each case, the ego-CAV enters the eco-approach region at different signal time to encounter most signal timings at the intersection. In each setting, forty times simulations are conducted with different random seeds to provide stochastic traffic states.

The proposed controller: The proposed controller is capable of eco-approaching towards an isolated actuated signal timing.

The baseline: The baseline is a Human-driven Vehicle (HV). It follows the Wiedemann car following model imbedded in the VISSIM platform (Fan et al., 2013). It computes motion commands by equation (27).

$$a_{ego} = \frac{1}{2} \times \frac{\Delta v^2}{\Delta s_{min} - (\Delta s - L_{front})} + a_{front} \tag{27}$$

where Δv is the speed difference between the ego-vehicle and the preceding vehicle; Δs is the distance between the two vehicles; Δs_{min} is the minimum following distance; L_{front} is the length of the preceding vehicle; a_{front} is the acceleration of the preceding vehicle; a_{ego} is the acceleration of the ego-vehicle.

3.3. Measures of effectiveness

There are five types of Measures of effectiveness (MOEs).

Function validation: The function of eco-approach via catching the potential passing time window is quantified by vehicle sample trajectories. Two scenarios are specifically illustrated to highlight the strengthen of the proposed method. *Scenario (I)*: ego-vehicle arrives at the end of a green signal. *Scenario (II)*: ego-vehicle arrives at the end of a red signal.

Passing time window prediction capability: The capability of predicting passing time window is evaluated by real-time prediction of signal switching time. In this research, signal switching time is predicted as the time when the cumulative probability of signal switching is greater than 0.5, indicating the risk parameter γ is set to 0.5 in equation (21). Moreover, the capability of predicting passing time window is quantified by the prediction error $e_{\mathbf{K}_{pass}}$ that is defined as equation (28).

$$e_{\mathbf{K}_{pass}} = |\widetilde{k}_{sw} - k_{sw}|\Delta\tau \tag{28}$$

where $\widetilde{k}_{sw}$ is the predicted signal-switching step; k_{sw} is the real signal-switching step. The signal switching time is the boundary of passing time window, according to the definition of passing time window in equation (12).

Fuel efficiency: This MOE is quantified by two indexes: fuel consumption and stop count. The fuel consumption is calculated by VT-micro model (Rakha et al., 2004), and the parameters of this model were previously calibrated by the authors. The correlation among speed, acceleration, and fuel consumption is depicted in Fig. 8.

Driving mobility: This MOE is quantified by the travel time. Travel time is defined as the duration from the initiation of the eco-approach maneuver to the moment the vehicle crosses the stop line.

Driving safety: This MOE is quantified by the minimum Time-to-Collision (TTC).

Computational efficiency: This MOE is quantified by the computation time.

3.4. Results

The results confirm the effectiveness of the proposed controller in several aspects: i) It effectively performs an eco-approach to an actuated signalized intersection. ii) The controller demonstrates the ability to predicting passing time window with an accuracy of within 3.1 s iii) It improves fuel efficiency by 9.1%. iv) The controller reduces the number of stops by 14.8%. v) It results in only 5.5 s of additional travel time. vi) The proposed controller enhances safety performance by 78.43%. vii) The computational efficiency is maintained at 12 ms.

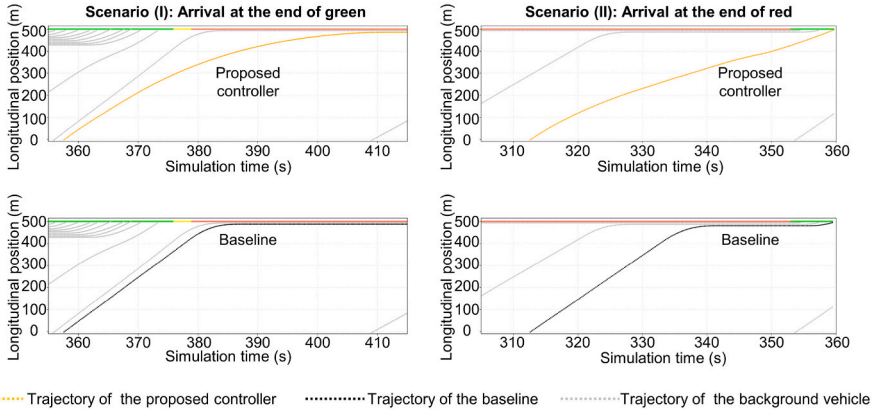

Fig. 9. Vehicle trajectories towards an isolated actuated signalized intersection.

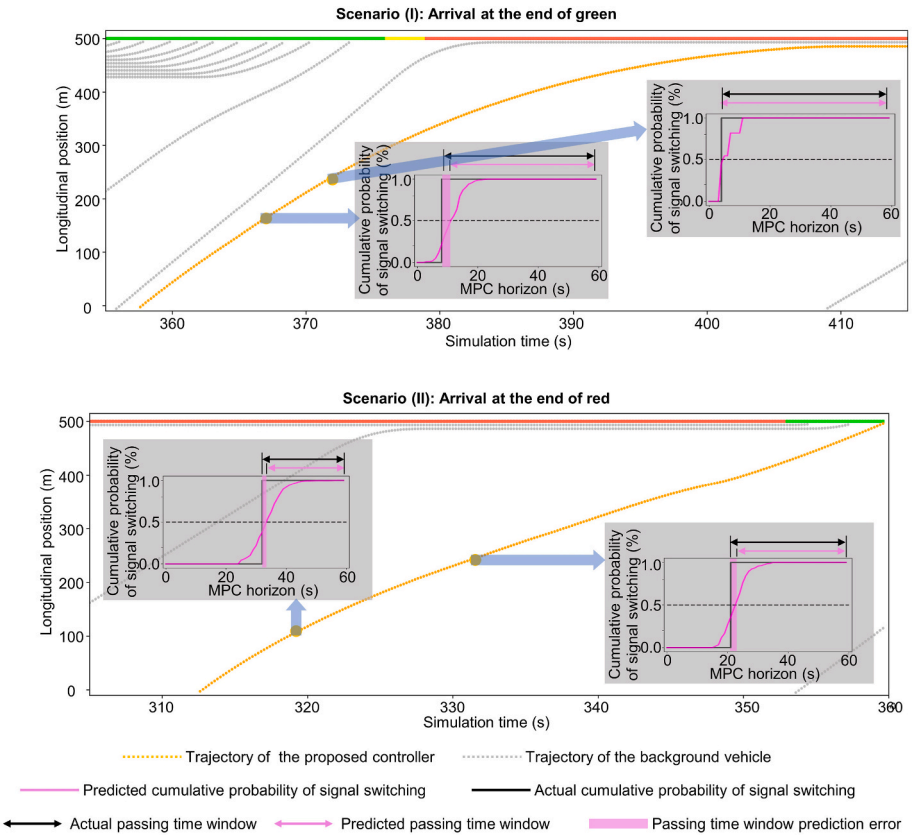

Fig. 10. Real-time prediction of passing time window: cumulative probability of signal switching time.

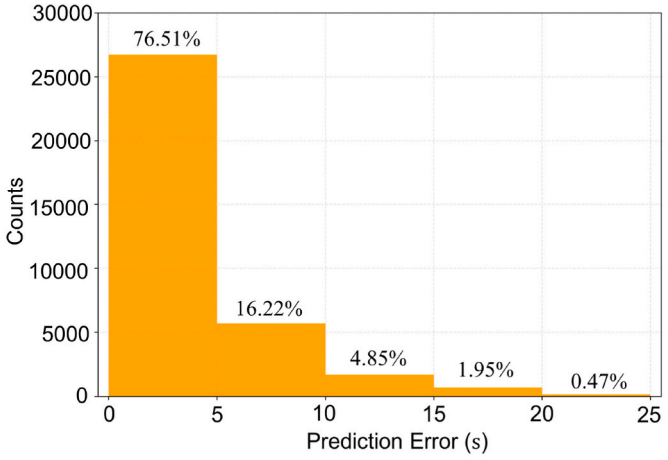

Fig. 11. Distribution of prediction error for passing time window.

3.4.1. *Function validation*

Vehicle sample trajectories are captured and depicted in Fig. 9, effectively showcasing the comparison between the proposed controller and the baseline. In Scenario (I), illustrated by Fig. 9-(I), the proposed controller demonstrates an eco-friendly approach by slowing down when it identifies no opportunity for passing. In stark contrast, the baseline controller abruptly applies brakes and comes to a stop before the stop-line. In Scenario (II), illustrated by Fig. 9-(II), the proposed controller exhibits its capability to intelligently utilize the start of the green light, while the baseline method stops at the stop-line, waiting for a green signal. The proactive behaving thereby enhances the fuel efficiency of the proposed method, reducing fuel consumption by 18.2% in Scenario (I) and 16.7% in Scenario (II).

3.4.2. *Passing time window prediction capability*

Signal switching time is the boundary of passing time window. Results of signal switching time prediction in the Scenario (I) and Scenario (II) are presented in Fig. 10. Results show that in the two scenarios, the average prediction error is 1.1 s. The prediction of signal switching time

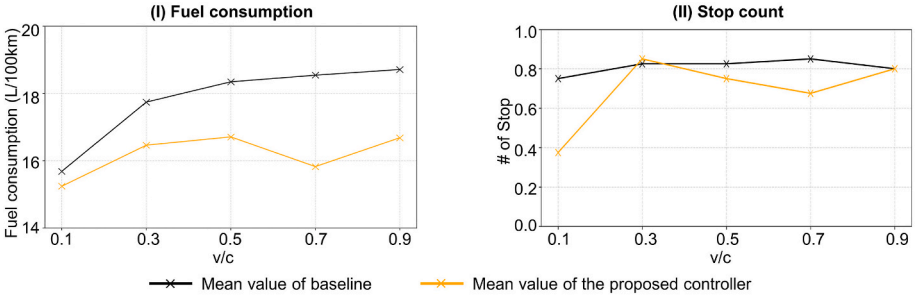

Fig. 12. Sensitivity analysis for ego-vehicle's fuel efficiency.

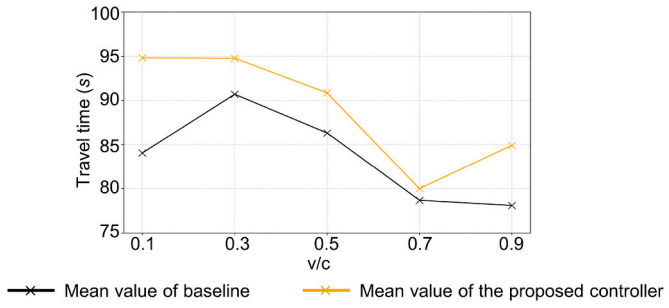

Fig. 13. Sensitivity analysis for driving mobility.

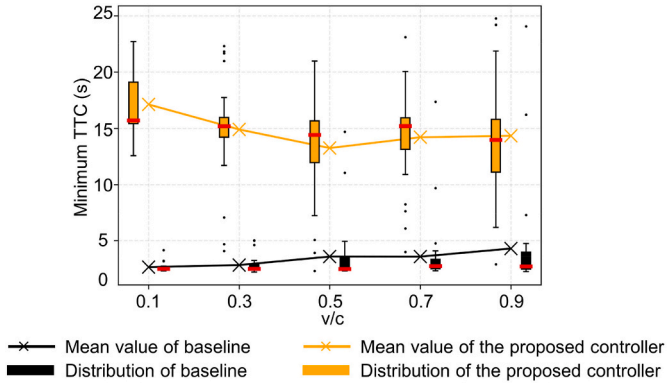

Fig. 14. Sensitivity analysis for driving safety.

agrees well with actual experiment results. The prediction capability of passing time windows is quantified in Fig. 11. The analysis reveals that the average prediction error amounts to 3.1 s, with a median error of 2 s. Additionally, the proposed method ensures that 76.5% of predictions exhibit errors of less than 5 s and 92.7% of predictions are within 10 s of accuracy. This confirms that the proposed controller is capable of ensuring an accurate prediction of passing time window.

3.4.3. Fuel efficiency

The fuel efficiency of the proposed controller is assessed by analyzing ego-vehicle's fuel consumption and the number of stops. Statistical analysis reveals that the proposed controller reduces fuel consumption by 9.1% and stop count by 14.8%, compared to conventional HVs. To further investigate the fuel efficiency across different congestion levels, a sensitivity analysis is conducted.

Fig. 12-(I) presents the results of the sensitivity analysis on ego-vehicle's fuel consumption, demonstrating consistent fuel consumption reductions across various v/c ratios. The observed trend in fuel consumption concerning v/c ratios makes sense, as both HVs and the proposed controller generally experience increased fuel consumption with higher congestion levels. Notably, there is a slight enhancement in fuel consumption around v/c = 0.7 for the proposed controller. This result aligns with the concept that the ego-vehicle has a higher likelihood of catching green lights in denser traffic, thanks to longer green phases allocated. However, in extremely congested traffic conditions (v/c = 0.9), the ego-CAV cannot catch the green light anymore, due to a high number of obstructing vehicles. Similar trend could be found in the analysis of stop count, as illustrated in Fig. 12-(II). The proposed controller exhibits fewer stops compared to the baseline HV across all congestion levels. The reduction of stop count is particularly notable in uncongested traffic conditions. However, in highly congested traffic (v/c = 0.9), the proposed controller cannot significantly reduce stop counts anymore.

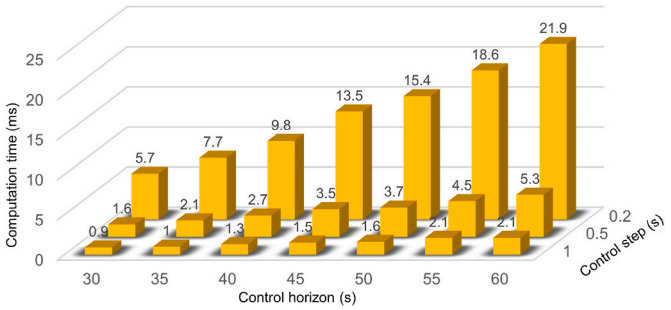

Fig. 15. The computation time regarding varying parameter settings.

3.4.4. Driving mobility

The impact of the proposed controller on driving mobility is assessed primarily through travel time. Statistical analysis shows that the proposed controller slightly enhances travel time by 6.6%, about 5.5 s. To gain a comprehensive understanding of its effects across varying congestion levels, a sensitivity analysis is conducted, as depicted in Fig. 13. This analysis reinforces the observation that the proposed controller may lead to a minor reduction in driving mobility. Moreover, an analysis of the trend reveals that travel time for both the baseline and the proposed controller slightly decreases with increasing v/c ratio. However, it's noteworthy that when v/c = 0.7, the proposed controller exhibits nearly equivalent mobility performance to the baseline. Conversely, its mobility decreases when v/c = 0.9. These findings align with the results observed in the sensitivity analysis for fuel consumption. This observation suggests that the proposed controller is optimally effective when implemented in scenarios where the v/c is 0.7.

3.4.5. Driving safety

The driving safety of the ego-vehicle is assessed using the minimum TTC, as illustrated in Fig. 14. This figure demonstrates that the proposed controller significantly improves the average minimum TTC by 317.14%, elevating it from 3.5 s in the baseline to 14.6 s with the implementation of the proposed controller. Furthermore, the minimum value of the minimum TTC under the proposed controller is recorded at 2.3 s, which is also greater than the baseline value of 2.1 s. The evaluation demonstrates that the proposed controller maneuvers a vehicle more conservatively to ensure driving safety.

3.4.6. Computational efficiency

Computational efficiency is quantified by the average computation time, as illustrated in Fig. 15. It demonstrates that the average computation time is 12 ms across all settings. The proposed controller can ensure a computation time within 20 ms in nearly all cases. It indicates that the proposed controller is ready for real-time applications.

3.4.7. Parameter tuning

The risk parameter γ in equation (21) represents the cumulative probability of signal switching. This parameter's tuning significantly influences the prediction accuracy of the passing time window, which in turn affects the overall efficiency of the eco-approach controller. To elucidate this relationship, a sensitivity analysis was conducted with varying risk parameter settings.

As shown in Fig. 16-(I), the average prediction error of the passing time window demonstrates a nonmonotone relationship with the risk parameter: initially decreasing and subsequently increasing as the parameter value rises. The most accurate prediction occurs when the risk parameter is set at 0.5. This observation is logical as a cumulative probability of signal switching set at 0.5 represents the mean and most probable time for signal transition.

Fig. 16-(II) illustrates the relationship between the risk parameter and variations in the fuel consumption and travel time of the ego-vehicle. This figure reveals that fuel consumption initially decreases

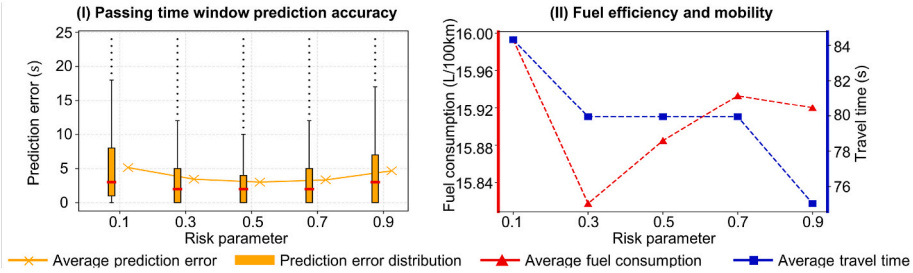

Fig. 16. Risk parameter tuning.

with a risk parameter below 0.3, then increases for parameters between 0.3 and 0.7, followed by a slight decrease when the parameter exceeds 0.7. Conversely, travel time consistently decreases as the risk parameter increases, although the reduction in travel time is less pronounced when the parameter is between 0.3 and 0.7.

These patterns can be interpreted as follows: A higher risk parameter generally signifies a more aggressive driving style during green lights and a more conservative approach during red lights. Aggressive driving in green phases aids in catching the end of the green light, potentially reducing waiting times at intersections. This behavior contributes significantly to decreased travel times (as indicated by the blue line in Fig. 16-(II)) and reduced fuel consumption (as shown by the red line in Fig. 16-(II) for risk parameters below 0.3 and above 0.7). On the other hand, conservative driving during red phases can lead to unnecessary slowing down, resulting in increased fuel consumption (as observed in the red line in Fig. 16-(II) for risk parameters between 0.3 and 0.5).

Consequently, the risk parameter in this research is set at 0.5, prioritizing fuel efficiency over mobility while achieving optimal prediction accuracy. This setting also lays a foundation for practical application, allowing users to tailor the risk parameter based on their preferences and driving conditions, as depicted in Fig. 16 For instance, setting the risk parameter to 0.3 optimizes fuel efficiency, while a setting of 0.9 maximizes mobility. Such customization offers flexibility in adapting the eco-approach strategy to individual needs and traffic scenarios.

4. Conclusion and future research

This research proposes an optimal control based eco-approach method. It enables an eco-approach towards an actuated signalized intersection. The proposed method bears the following features: i) capable of predicting the ever-changing actuated signal timing; ii) with enhanced fuel efficiency via proactively catching feasible passing time window; iii) with real-time computation efficiency for implementation. An evaluation has been conducted. Results demonstrate that:

- The average prediction error of passing time window is 3.1 s. Moreover, the proposed method has a chance of 76.5% to predict a passing time window within an error of 5 s.
- The proposed method enhances fuel efficiency by 9.1%, reduces stop count by 14.8%, and enhances driving safety by 317.14%, compared to the conventional human-driven vehicle.
- The proposed method fully leverages its strength when v/c is 0.7.
- A risk parameter setting of 0.3 yields optimal fuel efficiency, 0.9 provides the best mobility, and 0.5 achieves the highest prediction accuracy.
- The proposed method boasts a rapid computation of 12 ms, demonstrating its readiness for field implementation.

This research enables a vehicle to eco-approach an isolated signalized intersection with the capability of predicting actuated signal timing. Future studies could consider enhancing the proposed work in terms of its compatibility with multiple consecutive intersections. Moreover, the improvement of vehicle trajectory prediction represents a promising avenue for the performance enhancement of the proposed work.

CRediT authorship contribution statement

Jia Hu: Conceptualization, Funding acquisition, Project administration, Supervision. **Shuoyuan Li:** Data curation, Formal analysis, Investigation, Software, Writing – original draft. **Haoran Wang:** Conceptualization, Funding acquisition, Methodology, Supervision, Writing – original draft, Writing – review and editing. **Ziran Wang:** Resources, Validation, Visualization, Writing – review and editing. **Matthew J. Barth:** Resources, Supervision, Writing – review and editing.

Declaration of competing interest

The authors declare the following financial interests/personal relationships which may be considered as potential competing interests: Jia Hu reports financial support was provided by National Key R&D Program of China. Jia Hu reports financial support was provided by Shanghai Automotive Industry Science and Technology Development Foundation. Jia Hu reports financial support was provided by Tongji Zhongte Chair Professor Foundation. Haoran Wang reports financial support was provided by Shanghai Rising-Star Program. Haoran Wang reports financial support was provided by Shanghai Post-doctoral Excellence Program. Haoran Wang reports financial support was provided by China Postdoctoral Science Foundation.

Data availability

The data that has been used is confidential.

Acknowledgment

This paper is partially supported by National Key R&D Program of China (No. 2022ZD0115503), National Natural Science Foundation of China (No. 52302412 and 52372317), Shanghai Automotive Industry Science and Technology Development Foundation (No. 2213), Tongji Zhongte Chair Professor Foundation (No. 000000375–2018082), Shanghai Sailing Program (No. 23YF1449600), Shanghai Post-doctoral Excellence Program (No.2022571), and China Postdoctoral Science Foundation (No. 2022M722405).

Appendix. List of Symbols

Indices	Definition
a_k	The acceleration of ego-CAV (m/s^2)
a_{min}	The minimum accelerations of eco-CAV (m/s^2)
a_{max}	The maximum accelerations of eco-CAV (m/s^2)
$\boldsymbol{A}$	The coefficient matrix of the state vector in system dynamics
A_k^G	Defining the event A_k^G as observing a green light at step k
$\overline{A}_{k_{sw}}^G$	The opposite event that the signal is not green at step k_{sw}
$\boldsymbol{B}$	The coefficient matrix of the control vector in system dynamics
cap_J	The road capacity of the J entry of the intersection.
D_{eco}	Distance for eco-approach (m)
$\widetilde{\boldsymbol{D}}_k$	A concomitant matrix in the solution algorithm
$e_{\mathbf{K}_{pass}}$	The prediction error of passing time window
$G_{\varphi_j}^{min}$	Minimum green time of the φ_j signal phase (s)
$G_{\varphi_j}^{max}$	Maximum green time of the φ_j signal phase (s)
$\boldsymbol{G}_k$	A concomitant matrix in the solution algorithm
$H^{x_*(t)}$	The number of occurrences of $x_*(t)$ in the historical data set, $* \in \{s, c_i\}$
$H_{x_*(t+\lambda)}^{x_*(t)}$	The number of transitions from $x_*(t)$ to $x_*(t+\lambda)$ in the historical data set, $* \in \{s, c_i\}$
$\boldsymbol{H}_k$	A concomitant matrix in the solution algorithm
i	The index of the cell, $i \in \{0, 1, 2, \ldots, N\}$
$iter$	Iteration index in the solution algorithm
j	The index of signal phase, $j \in \{1, 2, 3, 4\}$
J	The index of intersection approach, $J \in \{east, south, west, north\}$
k	The control step index
K	The number of total control steps
$\widetilde{K}$	The signal time of the prediction horizon
k_{sw}	The signal-switching step
$\widetilde{k}_{sw}$	The predicted signal-switching step
$\mathbf{K}_{pass}$	A collection of planning steps ahead of or after the signal-switching step
N	The number of cells
$p_{t+\Delta t}^G$	The probability of observing a green light after time duration Δt
$p_{k_{sw}}^S$	The signal-switching probability at a specific step
$p_{K_{sw}}^S$	The probability of signal switching event occurring within the K_{sw} steps
$\boldsymbol{P}_k$	A concomitant matrix in the solution algorithm
q_v	The weighting factor of longitudinal speed error cost
q_J	The volume of the vehicle from J entry of the intersection.
$\boldsymbol{Q}$	The weighting factor of state error cost
$\widetilde{\boldsymbol{Q}}_k$	A concomitant matrix in the solution algorithm
r_a	The weighting factor of acceleration cost
R	The weighting factor of control cost
s_k^{front}	The longitudinal position of the preceding vehicle at step k (m)
s_{safe}	The minimum safe following gap (m)
s_{stop}	The longitudinal position of the stop-line (m)
s_k	The longitudinal position of ego-CAV (m)
$\boldsymbol{S}_k$	A concomitant matrix in the solution algorithm
t	The signal time, $t \in \{0, 1, 2, \ldots, T-1\}$
Δt	The transition horizon
T	The length of a signal cycle (s)
T_A	Duration of yellow (s)
T_r	Duration of red clearance (s)
$\boldsymbol{T}_k$	A concomitant matrix in the solution algorithm
u_k	The system control vector
v_k	The speed of ego-CAV (m/s)
v_{max}	The speed limit (m/s)
$x_{c_i}(t)$	The state of the ith cell at signal time t
$x_s(t)$	The state of the signal phase at signal time t
$\boldsymbol{\xi}^R$	Roadside state
$\boldsymbol{\xi}_k^V$	Onboard vehicle state
$\boldsymbol{\xi}_{des,k}^V$	The desired vehicle state at step k
$\pi_{\boldsymbol{\xi}^R(t+\Delta t)}^{\boldsymbol{\xi}^R(t)}$	The transition probability of roadside state from $\boldsymbol{\xi}^R(t)$ to $\boldsymbol{\xi}^R(t+\Delta t)$
$\Delta\tau$	The length of the control step (s)
φ_j	The j signal phase
γ	Risk parameter, $\gamma \in (0, 1)$

References

Aminzadegan, S., Shahriari, M., Mehranfar, F., Abramović, B., 2022. Factors affecting the emission of pollutants in different types of transportation: a literature review. Energy Rep. 8, 2508–2529.

Borek, J., Groelke, B., Earnhardt, C., Vermillion, C., 2022. Hierarchical control of heavy-duty trucks through signalized intersections with non-deterministic signal timing. IEEE Trans. Intell. Transport. Syst. 23 (8), 13769–13781.

Davis, S.C., Boundy, R.G., 2021. Transportation Energy Data Book: Edition 39. Oak Ridge National Lab.(ORNL), Oak Ridge, TN (United States).

Dong, H., Zhuang, W., Chen, B., Lu, Y., Liu, S., Xu, L., Pi, D., Yin, G., 2022. Predictive energy-efficient driving strategy design of connected electric vehicle among multiple signalized intersections. Transport. Res. C Emerg. Technol. 137, 103595.
Dong, H., Zhuang, W., Chen, B., Yin, G., Wang, Y., 2021. Enhanced eco-approach control of connected electric vehicles at signalized intersection with queue discharge prediction. IEEE Trans. Veh. Technol. 70 (6), 5457–5469.
Fan, R., Yu, H., Liu, P., Wang, W., 2013. Using VISSIM simulation model and Surrogate Safety Assessment Model for estimating field measured traffic conflicts at freeway merge areas. IET Intell. Transp. Syst. 7 (1), 68–77.
Fei Ye, P.H., Guoyuan, Wu, Danial, Esaid, Kanok, Boriboonsomsin, Matthew, Barth, 2019. Deep learning-based queue-aware eco-approach and departure system for plug-in hybrid electric bus at signalized intersections: a simulation study. In: Advances and Current Practices in Mobility.
Gagniuc, P.A., 2017. Markov Chains: from Theory to Implementation and Experimentation. John Wiley & Sons.
Guo, Q., Angah, O., Liu, Z., Ban, X., 2021. Hybrid deep reinforcement learning based eco-driving for low-level connected and automated vehicles along signalized corridors. Transport. Res. C Emerg. Technol. 124.
Hao, P., Wu, G., Boriboonsomsin, K., Barth, M.J., 2019. Eco-approach and departure (EAD) application for actuated signals in real-world traffic. IEEE Trans. Intell. Transport. Syst. 20 (1), 30–40.
Holmberg, K., Andersson, P., Erdemir, A., 2012. Global energy consumption due to friction in passenger cars. Tribol. Int. 47, 221–234.
Hu, J., Lei, M., Wang, H., Wang, M., Ding, C., Zhang, Z., 2023. Lane-level navigation based eco-approach. IEEE Transactions on Intelligent Vehicles 8 (4), 2786–2796.
Hu, J., Zhang, Z., Xiong, L., Wang, H., Wu, G., 2021. Cut through traffic to catch green light: eco approach with overtaking capability. Transport. Res. C Emerg. Technol. 123.
Jia, H., Hao-ran, W., Yong-wei, F., Xin, L., 2022. An optimal control based motion planner in mixed-domain. China J. Highw. Transp. 35 (3), 43.
Lei, Z., Cai, J., Li, J., Gao, D., Zhang, Y., Chen, Z., Liu, Y., 2023. Hierarchical eco-driving control for plug-in hybrid electric vehicles under multiple signalized intersection scenarios. J. Clean. Prod. 420.
Li, Y., 2017. Deep Reinforcement Learning: an Overview arXiv preprint arXiv: 1701.07274.
Masson-Delmotte, V., Zhai, P., Pörtner, H.-O., Roberts, D., Skea, J., Shukla, P.R., 2022. Global Warming of 1.5° C: IPCC Special Report on Impacts of Global Warming of 1.5° C above Pre-industrial Levels in Context of Strengthening Response to Climate Change, Sustainable Development, and Efforts to Eradicate Poverty. Cambridge University Press.
Rakha, H., Ahn, K., Trani, A., 2004. Development of VT-Micro model for estimating hot stabilized light duty vehicle and truck emissions. Transport. Res. Transport Environ. 9 (1), 49–74.
Shafik, A.K., Eteifa, S., Rakha, H.A., 2023. Optimization of vehicle trajectories considering uncertainty in actuated traffic signal timings. IEEE Trans. Intell. Transport. Syst. 24 (7), 7259–7269.
Shin, J., Sunwoo, M., 2018. Vehicle speed prediction using a Markov chain with speed constraints. IEEE Trans. Intell. Transport. Syst. 20 (9), 3201–3211.
Sun, C., Guanetti, J., Borrelli, F., Moura, S.J., 2020. Optimal eco-driving control of connected and autonomous vehicles through signalized intersections. IEEE Internet Things J. 7 (5), 3759–3773.
Vindula Jayawardana, C.W., 2022. Learning Eco-Driving Strategies at Signalized Intersections, 2022 European Control Conference (ECC). London, United Kingdom.
Wang, H., Hao, W., So, J., Xiao, X., Chen, Z., Hu, J., 2023. A faster cooperative lane change controller enabled by formulating in spatial domain. IEEE Transactions on Intelligent Vehicles.
Wang, H., Hu, J., Feng, Y., Li, X., 2022a. Optimal control-based highway pilot motion planner with stochastic traffic consideration. IEEE Intell. Transp. Syst. Mag. 15 (1), 421–436.
Wang, H., Lai, J., Zhang, X., Zhou, Y., Li, S., Hu, J., 2022b. Make Space to Change Lane: A Cooperative Adaptive Cruise Control Lane Change Controller, vol. 143. Transportation Research Part C: Emerging Technologies.
Wang, H., Li, X., Zhang, X., Hu, J., Yan, X., Feng, Y., 2022c. Cut through traffic like a snake: cooperative adaptive cruise control with successive platoon lane change capability. Journal of Intelligent Transportation Systems.
Wang, H., Wang, X., Li, X., Wu, X., Hu, J., Chen, Y., Liu, Z., Li, Y., 2022d. A pathway forward: the evolution of intelligent vehicles research on IEEE T-IV. IEEE Transactions on Intelligent Vehicles 7 (4), 918–928.
Yang, Y., Ma, F., Wang, J., Zhu, S., Gelbal, S.Y., Kavas-Torris, O., Aksun-Guvenc, B., Guvenc, L., 2020. Cooperative ecological cruising using hierarchical control strategy with optimal sustainable performance for connected automated vehicles on varying road conditions. J. Clean. Prod. 275, 123056.
Zhang, J., Jiang, X., Cui, S., Yang, C., Ran, B., 2022. Navigating electric vehicles along a signalized corridor via reinforcement learning: toward adaptive eco-driving control. Transport. Res. Rec. 2676 (8), 657–669.